MULTIAXIAL FATIGUE STUDIES ON CARBON STEEL PIPING MATERIAL OF INDIAN PHWRS

Punit Arora[1], Suneel. K. Gupta [1], V.Bhasin[1], K.K. Vaze[1], S. Sivaprasad [2] and S. Tarafdar [2]
[1]Bhabha Atomic Research Centre, Mumbai 400 085, India
[2]National Metallurgical Laboratory, Jamshedpur 831 001, India
Email of corresponding author: punit@barc.gov.in

ABSTRACT

The tests studies and analyses have been carried out in the area of "Multiaxial Fatigue" with an objective to improve the damage assessment methodologies and design rules. Nearly 50 numbers of fatigue tests were conducted on solid and tubular specimens of SA333Gr.6 material under pure axial, pure shear and combined axial-torsion in-phase/ out-of-phase loading combinations. A software has been developed for the evaluation of multiaxial fatigue damage for the analyses of tests data using different invariant fatigue models such as ASME Sec.III code procedures, von-Mises etc. The fatigue crack initiation life was predicted using the best fit axial fatigue life curve (without use of safety factors). These tests and their analyses have helped in understanding the fatigue failure behavior of piping material under complex cyclic loadings where the principal directions rotate during a loading cycle. The crack initiation angles have also been measured by analyzing the image of the tested specimens. The measured crack angles will help in validation of the critical plane based models.

INTRODUCTION

Power Plant Mechanical Components (PPC) such as piping, vessels etc. are subjected to periodic cyclic loading during its normal operation, as well as during the design basis accident events, and mainly fails due to the fatigue cracking. Generally the fatigue damage is evaluated according to the design codes, which use fatigue design curves and a linear damage accumulation hypothesis. The fatigue design curves are derived from material's uniaxial fatigue tests. However, due to complex geometry and loadings on a component, the state of induced stresses / strains is multiaxial and non-proportional due to varying principle directions.

In view of above, systematic experimental and analytical studies have been carried on specimens made of low carbon manganese steel conforming to ASME specification of SA-333 Gr.6. The material specifications of this steel are same as used in Indian Pressurized Heavy Water Reactor's (PHWR) Primary Heat Transport (PHT) piping. The various types of tests conducted are, monotonic tensile, tension compression that is axial fatigue tests on solid specimens, pure torsion fatigue tests on tube specimen, in-phase axial-torsion fatigue tests on tube specimens and out of phase axial-torsion fatigue tests on tube specimens. All these tests were conducted at room temperature and in air environment. The results of these tests have been investigated in details, to understand and model the material's fatigue damage under multiaxial and non-proportional loading condition.

Large numbers of proposals for multiaxial fatigue analyses were developed in past and are available in literature [2-9], design codes [1] and text books. The state of the art of various fatigue models has been investigated which varies mainly as a function of the fatigue life and is different for low-cycle fatigue and high-cycle fatigue regions. These models have used different definitions for Fatigue Damage Parameter (FDP) and mostly these are based on the macro parameters such as stresses, strains, their invariants or strain energy or multiple of stress and strain. Literature show that the critical plane based models can provide information of the plane of the fatigue crack initiation. In the critical plane models the FDP uses resolved stresses / strains (normal and shear components) on the critical plane. The critical plane is obtained by maximizing a parameter such as shear stress or shear strain or FDP etc by rotating the oblique plane. However, the present study uses invariant based fatigue models and the well established design procedures such as ASME for the prediction of fatigue life.

EXPERIMENTAL DETAILS AND RESULTS

The fatigue experiments were conducted on standard solid cylindrical specimens and tubular specimens. The specimens were fabricated from the pipe made of SA333 Gr.6 (low carbon manganese steel). The chemical composition of the material is given in Table 1. The typical microstructure of SA 333 Gr. 6 material in as received condition shows the banded pearlite and ferrite phases (Fig. 1). Uniaxial monotonic tests were carried out to determine tensile properties of SA333 Gr.6 material. Two numbers of tests were conducted under quasi-static displacement control loading on the standard specimens. The specimens were

fabricated in accordance with requirements of ASTM E08. The tensile properties as evaluated from these tests are given in Table 2.

The tests were grouped into four categories, namely pure axial, pure shear, in-phase axial-torsion and out of phase axial-torsion with phase shifts of 90°, 45° and 180°. These tests have been conducted to investigate the effect of multiaxiality and rotation of principle stress axes (non-proportionality) on fatigue life.

Table 1: Chemical properties in weight percentage

C	Mn	Si	P	S	Cr	Ni	N	Balance
0.14	0.9	0.25	0.016	0.018	0.08	0.05	0.01	Fe

Table 2: Tensile properties of SA 333 Gr. 6 material

E (GPa)	σ_y (Mpa)	σ_u (Mpa)	%El
203	302	450	36.7

σ_y: yield strength, σ_u: Tensile strength, %El: percentage elongation

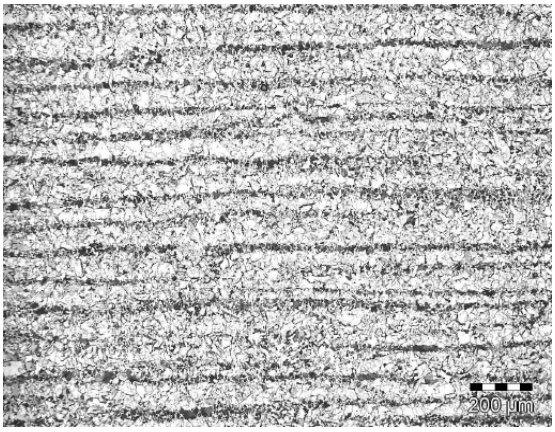

Fig. 1: The typical microstructure of SA 333 Gr 6 material in as received condition

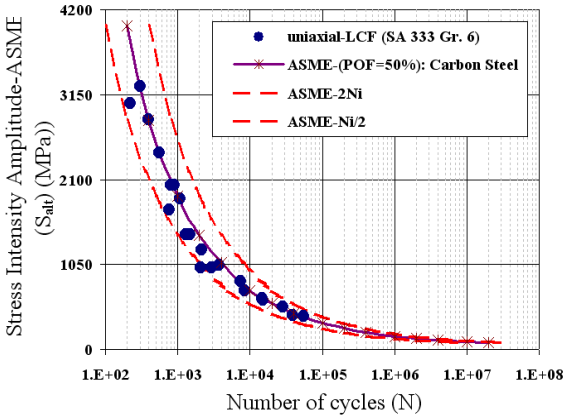

Fig. 2: The comparison between the fatigue failure curve of SA 333 Gr6 and ASME best fit curve

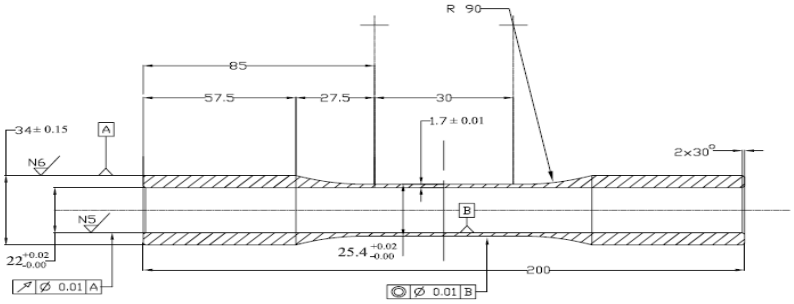

Fig. 3: Drawing of the tubular specimen

Axial Fatigue Tests on Solid Specimens

The solid specimen tests were conducted in a 100 kN closed loop servo-hydraulic test machine. The specimens were machined and tested as per the standard procedure of ASTM E 606. The tests were conducted under axial strain controlled conditions. The uniaxial fatigue failure tests data points as obtained from Low Cycle Fatigue (LCF) tests conducted on solid specimens has been plotted in Fig. 2.

The ASME Code fatigue design curves, given in Appendix I of Section III, are based on strain–controlled tests of small polished specimens at room temperature in air environment. The design fatigue curves have been developed from the best–fit (or median fit corresponding to Probability of Failure (POF) as 50%) curves obtained from experimental strain–vs.–life (ε–N) data and then reducing the fatigue life at each point on the best-fit curve by a factor of 2 on strain (or stress) or 20 on cycles. The factor of safety takes care of the uncertainties in loading, fatigue data scatter, size effect, surface finish and influence of atmosphere on fatigue life.

In present study, all the fatigue tests were conducted on small size polished specimens in air environment and under controlled loadings. In order to account the possibility of data scatter, the bounding curves have been plotted with a factor of 2 on ASME best fit curve as shown in Fig 2. This Fig. shows that the pure axial LCF tests conducted on SA 333 Gr. 6 material fall within the permissible bounds for data scatter about ASME best fit curve.

Multiaxial Fatigue Tests on tubular specimens

The pure torsion and axial-torsion fatigue tests were conducted on tubular specimens under reversible controlled strain cycling on a servo hydraulic tension-torsion machine with axial capacity as ± 100kN and torsion as ± 1000Nm. The tubular specimens were fabricated as per standard test procedure of ASTM E 2207. The test specimen drawing has been shown in Fig. 3. The thickness of the tube specimen was taken on the lower bound side as prescribed in ASTM standard such that the effect of shear stress gradient in thickness direction is minimized. The test set up for pure torsion and axial-torsion tests has been shown in Fig. 4.

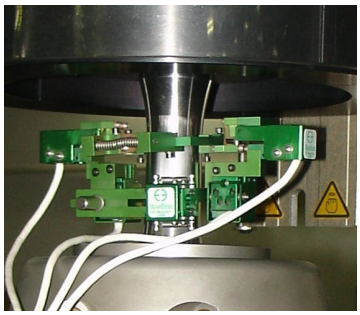

Fig. 4: The test set up for pure torsion and axial-torsion tests

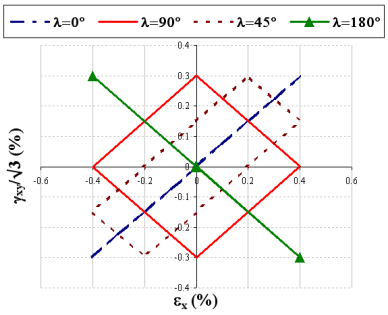

Fig. 5: Strain paths for 0°, 90°, 45° and 180° phase shifts axial-torsion tests

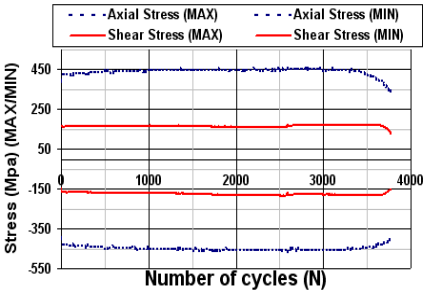

Fig. 6: Variation of maximum/ minimum axial and shear stress for ca40s52p45 test with load cycles

The pure torsion tests were aimed at generating reference data for material fatigue behavior under pure shear state of stress/strain. The axial-torsion fatigue tests were also conducted on tubular specimens under completely reversible axial and shear strain cycling. For axial-torsion fatigue tests, four loading paths, as shown in Fig. 5, have been used. The phase angle between the axial and shear strain cycle, have been varied that are, In-Phase (i.e. 0° Phase-Shift), 90°, 45° and 180° phase shifts. For each strain station of the shear and axial strain amplitudes, tests have been conducted under both In-Phase and 90° Phase-Shift condition. At few strain stations tests were also conducted with 45° and 180° phase shift angles. The typical variation of axial stress and shear stress versus number of load cycles has been shown in Fig. 6. The fatigue crack initiation life was defined with respect to 25% drop in load/ torque or a visible crack size, whichever is earlier.

Typical axial and shear stress-strain hysteresis loops, corresponding to half life of axial-torsion fatigue test with 0°, 90°, 45° and 180° phase-shifts, have been plotted in Figs. 7(a) and 7(b) respectively. This Fig clearly shows the extra hardening due to non-proportionality/ phase-shift in the loading. This can be related to extra fatigue damage in the material in terms of higher loop area for non-proportional loading. Further, the maxima and minima of stress and strain components exist at same time instant for proportional load condition indicating the synchronous behavior between stresses and strains. However, the maxima and minima of shear stress and strain do not occur at the same time instant under non-proportional loading condition (Fig. 7(b)). This signifies that the stress and strain are not synchronous to each other viz. there occurs independent rotation of principal stress and strain axes. This points to the complex nature of damage occurring under non-proportional load condition.

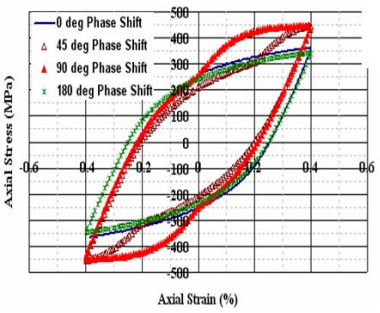

Fig. 7(a): Axial stress-strain hysteresis loop under different phase shifts

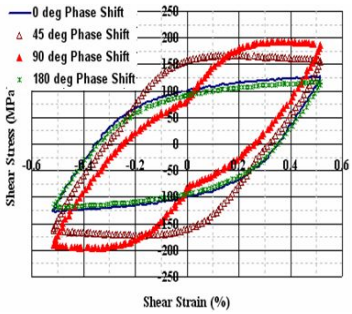

Fig. 7(b): Shear stress-strain hysteresis loop under different phase shifts

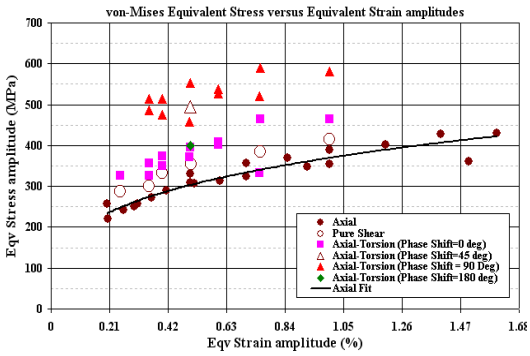

Fig. 8: von-Mises equivalent stress versus strain amplitude showing extra hardening in material for multiaxial stress state

The variation of von-Mises equivalent stress amplitude versus strain amplitude has been plotted in Fig. 8 for all the tests conducted under pure axial, pure torsion and axial-torsion tests conducted. The von-Mises equivalent stress and strain have been evaluated using equations (1) and (2) respectively. The Fig. 8 also shows the extra hardening in case of all multiaxial tests.

$$\sigma_{eq}^{a} = \left[\left(\sigma_{x}^{a} \right)^2 + 3 \left(\tau_{xy}^{a} \right) \right]^{1/2} \tag{1}$$

$$\varepsilon_{eq}^{a} = \frac{\sqrt{2}}{2(1+\upsilon')} \left[\left(\varepsilon_{x}^{a} - \varepsilon_{y}^{a} \right)^2 + \left(\varepsilon_{y}^{a} - \varepsilon_{z}^{a} \right)^2 + \left(\varepsilon_{z}^{a} - \varepsilon_{x}^{a} \right)^2 + 6 \left(\varepsilon_{xy}^{a} + \varepsilon_{yz}^{a} + \varepsilon_{zx}^{a} \right) \right]^{1/2} \tag{2}$$

where, υ' is the effective poisson's ratio and is given by equation (3).

$$\upsilon' = \frac{\upsilon^{el} \varepsilon_{eq}^{el} + \upsilon^{pl} \varepsilon_{eq}^{pl}}{\varepsilon_{eq}^{el} + \varepsilon_{eq}^{pl}}, \ \upsilon^{el} = 0.3 \ \textit{and} \ \upsilon^{pl} = 0.5 \tag{3}$$

The loading details and the number of cycles to fatigue crack initiation for multiaxial tests have been presented in Table 3. This table shows that in case of non-proportional load condition, fatigue life reduced by a factor of as high as 4 (refer tests ca30s46p0 and ca30s46p90 in Table 3) when compared with the fatigue life recorded in the corresponding proportional loading test. This could be due to the extra hardening in case of non-proportional load condition which causes addition fatigue damage in the material. Liu et. al. [10] have carried out the microstructure studies on aluminum alloy under transmission electron microscope (TEM) to investigate the effect of non-proportionality/ phase shift on dislocation sub-structures. It was examined that repetitive activation/ de-activation of the multiple slip systems under non-proportional tests causes the interaction of gliding dislocations on different slip planes leading to the formation of dislocation cross bands. The mobility of the dislocations further reduces leading to extra strain hardening in the material. This results in higher fatigue damage and reduction in fatigue life.

The specimen subjected to pure shear fatigue cycling failed with an axial crack in gauge region of tubular specimen as shown in Fig. 9 (a). However, combined axial-torsion loading resulted in an inclined crack as shown in Figs. 9(b) and 9(c).

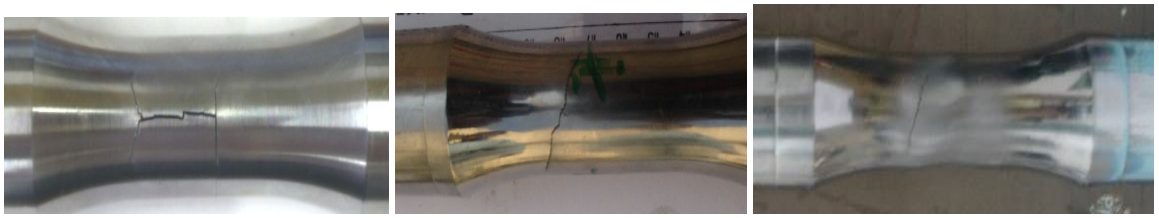

(a) (b) (c)

Fig. 9: (a) The axial crack appearing in pure torsion test, (b) inclined crack orientation in axial-torsion with 0^o phase shift and (c) inclined crack in axial-torsion test with 90^o phase shift angle

Measurement of crack angles

It is widely studied that fatigue crack initiation is caused by cyclic plasticity. The Persistent Slip Bands (PSB) are found to form in the grains which are closely aligned with the plane of maximum shear. Even near to the fatigue limit, there occurs the plastic strain of the amplitude nearly 10^{-5} due to the formation of PSBs. The critical plane models [2-9] are based on this realistic physical phenomenon of Persistent Slip Bands (PSB) and can be applied for fatigue life assessments. These models can also predict the maximum damage plane/ critical plane on which crack is more likely to initiate. In order to study/ validate such predictions for critical plane orientations, the crack angles (ϕ) (i.e. the angle between the axial direction and normal to crack plane as shown in schematic Fig. 10(b)) have been measured using post image analysis of the cracked specimens. Fig. 10(a) shows the measurement of the crack angle in a typical cracked tubular specimen. However, the investigations on the various critical planes based fatigue approaches are in progress.

In order to validate the crack initiation location by visual inspection, few of the specimens were cut open and studied under Scanning Electron Microscope (SEM). The typical SEM image has been shown in Fig. 10(c) indicating the crack initiation spots at outer diameter of the tested specimen which was initially located by visual inspection. However, the crack orientation measurement using image processing has been carried out on millimeter scale of the crack length. This treatment will be consistent with definition of fatigue crack initiation life criterion and the macroscopic continuum assumption adopted in almost all the critical plane models relating damage in terms of normal/ shear stress and strain values on various material planes.

Table 3. Loading and fatigue life details for pure axial, pure torsion, axial-torsion (In-phase) and axial-torsion (Out-of-phase) tests conducted on SA 333 Gr 6 material

Test Category	Test name	Stress Amplitude (Mpa)		Mean Stress (Mpa)		Strain Amplitude (%)		Mean Strain (%)		λ (°)	N_i
		σ^a_{xx}	τ^a_{xy}	σ^m_{xx}	τ^m_{xy}	ε^a_{xx}	$\varepsilon^a_{xy}=\gamma^a_{xy}/2$	ε^m_{xx}	$\varepsilon^m_{xy}=\gamma^m_{xy}/2$		
PURE AXIAL (PUSH-PULL)	**INDY P**	348.5	0	0	0	0.92	0	0	0	0	1090
	INDY Q	314	0	0	0	0.605	0	0	0	0	2160
	INDY K	306	0	0	0	0.515	0	0	0	0	3700
	INDY L	288.5	0	0	0	0.415	0	0	0	0	7505
	INDY M	272.5	0	0	0	0.36	0	0	0	0	8490
	INDY N	257	0	0	0	0.31	0	0	0	0	14900
	INDY O	242.5	0	0	0	0.26	0	0	0	0	28300
	INDY R	221	0	0	0	0.205	0	0	0	0	39600
	AMTL-1/R=-1	250	0	0	0	0.3	0	0	0	0	15173
	AMTL-2/R=-1	310	0	0	0	0.5	0	0	0	0	2924
	AMTL-3/R=-1	325	0	0	0	0.7	0	0	0	0	1306
	AMTL-4/R=-1	355	0	0	0	1	0	0	0	0	891
	AMTL-5/R=-1	360	0	0	0	1.5	0	0	0	0	222
	NML-1/R=-1	256.52	0	0	0	0.2	0	0	0	0	54927
	NML-2/R=-1	330.49	0	0	0	0.5	0	0	0	0	2107
	NML-3/R=-1	356.43	0	0	0	0.7	0	0	0	0	1487
	NML-4/R=-1	369.07	0	0	0	0.85	0	0	0	0	769
	NML-5/R=-1	389.19	0	0	0	1	0	0	0	0	801
	NML-6/R=-1	401.78	0	0	0	1.2	0	0	0	0	559
	NML-7/R=-1	428.18	0	0	0	1.4	0	0	0	0	397
	NML-8/R=-1	428.93	0	0	0	1.6	0	0	0	0	303
PURE SHEAR	**CA0S43**	8.39	165.69	-1.83	-0.75	0	0.215	0	0	0	70118
	CA0S61	31.63	171.91	-4.13	-6.36	0	0.305	0	0	0	12097
	CA0S69	10.36	191.98	0.44	-0.46	0	0.345	0	0	0	8664
	CA0S87	15.63	204.54	-2.10	-0.04	0	0.435	0	0	0	4678
	CA0S130	13.06	221.96	1.76	-0.63	0	0.65	0	0	0	1589
	CA0S173	39.25	237.85	-7.49	-1.68	0	0.865	0	0	0	817
PROPORTIONAL AXIAL-TORSION TESTS	**CA18S30p0**	248.25	121.79	-3.79	2.94	0.18	0.15	0	0	0	27414
	CA20S50p0	212.45	142.74	-9.09	-0.92	0.2	0.25	0	0	0	16050
	CA20S60p0	209.29	161.82	-9.03	-0.01	0.2	0.3	0	0	0	14280
	CA20S79p0	175.36	189.15	-13.7	1.35	0.2	0.395	0	0	0	6431
	CA25S43p0	272.53	133.25	-1.61	-6.99	0.25	0.215	0	0	0	12338
	CA30S46p0	308.50	121.20	-4.15	-5.20	0.3	0.23	0	0	0	6770
	CA30S90p0	246.79	188.36	-3.54	-1.02	0.3	0.45	0	0	0	2709
	CA40S52p0	336.05	119.67	-1.66	-1.13	0.4	0.26	0	0	0	3400
	CA42S74p0	312.09	145.56	-6.99	-15.1	0.42	0.37	0	0	0	3340
	CA50S150p0	290.76	209.92	-4.22	-2.93	0.5	0.75	0	0	0	797
	CA60S78p0	397.33	138.71	-4.81	-0.85	0.6	0.39	0	0	0	1525
NON-PROPORTIONAL AXIAL-TORSION TESTS	**CA20S50p90**	355.63	191.23	-6.05	-2.43	0.2	0.25	0	0	90	4769
	CA20S60p90	361.18	210.82	-1.13	-3.61	0.2	0.3	0	0	90	6767
	CA20S79p90	290.46	204.55	-1.11	-0.76	0.2	0.395	0	0	90	3035
	CA25S43P90	398.21	188.04	-1.27	-2.22	0.25	0.215	0	0	90	6182
	CA30S46P90	371.66	170.30	-1.45	-1.18	0.3	0.23	0	0	90	1760
	CA30S90P90	369.61	217.22	-1.01	-1.55	0.3	0.45	0	0	90	1838
	CA40S52p90	441.14	191.88	-1.22	-1.48	0.4	0.26	0	0	90	2460
	CA40S52P45	411.57	157.78	-2.48	-2.21	0.4	0.26	0	0	45	3774
	CA40S52P180	343.96	118.65	-0.88	-0.59	0.4	0.26	0	0	180	4506
	CA42S74P90	411.91	199.65	-3.01	-9.13	0.42	0.37	0	0	90	2092
	CA60S78p90	467.72	207.22	0.17	-0.21	0.6	0.39	0	0	90	1180

λ: phase shift angle, N_i is corresponding to the number of cycles for load/ torque drop by 25%.

ANALYTICAL PREDICTION METHODOLOGY: ASME DESIGN PROCEDURE

The ASME section III NB is based on the maximum shear stress (Tresca) theory and considers damage in terms of maximum value of stress intensity amplitudes. The multiaxial fatigue tests data have also been analyzed using the ASME procedure for constant-principal directions (that is proportional loading) and varying principal directions (or non-proportional loading) conditions. It may be noted that this ASME procedure is valid with pseudo elastic stress which reflects the actual strains at the material point. The pseudo

elastic (σ_{ij}^{pe}) stresses were evaluated from the applied strain tensor history $\varepsilon_{ij}(t)$ using the Lame's equations of elasticity as given by equation (4).

$$\sigma_{ij}^{pe}(t)=\lambda\varepsilon_{kk}(t)\delta_{ij}+2G\varepsilon_{ij}(t) \quad (4)$$

In above equation λ is Lame's constant and G is Shear modulus of elasticity. Based on the pseudo elastic stress tensor history, that is $\sigma_{ij}^{pe}(t)$, calculations for the alternating stress intensity are carried out.

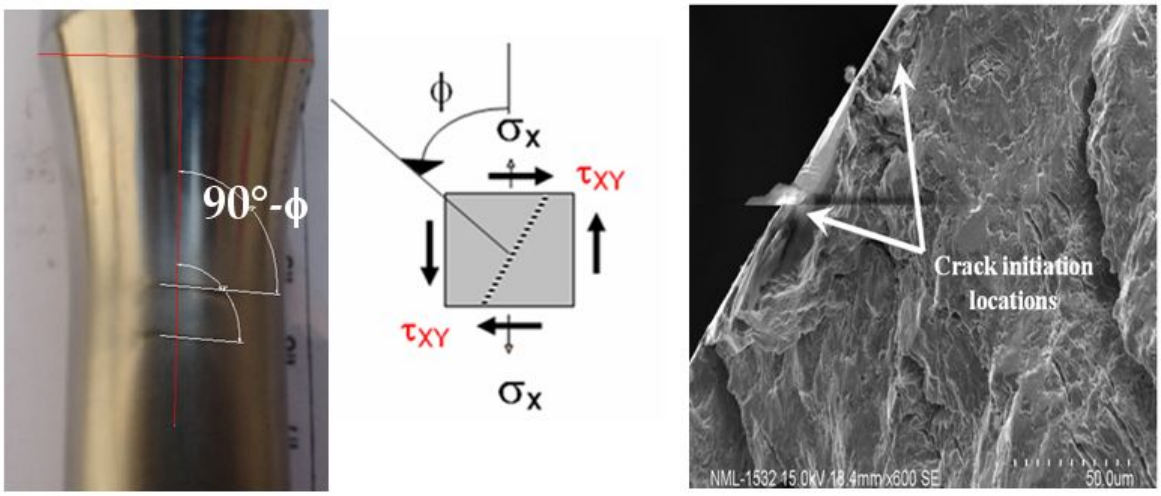

(a) (b) (c)

Fig. 10: (a) Measurement of crack angle (ϕ) in a typical cracked specimen, (b) schematic of material plane orientation and (c) SEM image of a typical cut-open test specimen indicating the crack initiation spots at outer surface

The procedures for assessment of fatigue crack initiation life under proportional loading and non-proportional loading are reproduced as below for ready reference,

Constant Principal Stress Directions (Proportional Loading)

- Evaluate the Principal Stresses for one load cycle. These are designated as $\sigma_1(t)$, $\sigma_2(t)$ and $\sigma_3(t)$.
- Determine the stress intensities ($S_{ij}(t)$) versus time for the complete load cycle i.e. $S_{12}(t)= \sigma_1(t)-\sigma_2(t)$, $S_{23}(t)= \sigma_2(t)-\sigma_3(t)$ and $S_{31}(t)= \sigma_3(t)-\sigma_1(t)$.
- Evaluate the absolute range for each stress intensity (ΔS_{ij}), find the maximum range amongst three stress intensity ranges and designate it as ΔS_{rij}.

i.e., $\Delta S_{rij}=\max[|\Delta S_{12}|,|\Delta S_{23}|,|\Delta S_{31}|]$

- The alternating stress intensity (S_{alt}) is half of the largest stress intensity range ΔS_{rij}.

Varying Principal Stress Directions (Non-Proportional Loading)

- Evaluate the six stress components at highly stressed point versus time for one complete cycle ($\sigma_x(t)$,$\sigma_y(t)$, $\sigma_z(t)$, $\tau_{xy}(t)$, $\tau_{yz}(t)$ and $\tau_{zx}(t)$).
- Choose a reference point in time domain and designate it as t_0. The stress components at this reference time are denoted by ($\sigma_x(t_0)$,$\sigma_y(t_0)$, $\sigma_z(t_0)$, $\tau_{xy}(t_0)$, $\tau_{yz}(t_0)$ and $\tau_{zx}(t_0)$).
- Evaluate the stress difference with respect to reference time such as,
  $\sigma'_x(t)= \sigma_x(t)- \sigma_x(t_0)$, $\sigma'_y(t)= \sigma_y(t)- \sigma_y(t_0)$ etc.
- Evaluate the Principal stresses ($\sigma'_1(t)$, $\sigma'_2(t)$, $\sigma'_3(t)$) from stress differences ($\sigma'_x(t_0)$,$\sigma'_y(t_0)$, $\sigma'_z(t_0)$, $\tau'_{xy}(t_0)$, $\tau'_{yz}(t_0)$ and $\tau'_{zx}(t_0)$). σ'_1
- Determine the stress intensities ($S'_{ij}(t)$): $S'_{12}(t)= \sigma'_1(t)-\sigma'_2(t)$, $S'_{23}(t)= \sigma'_2(t)-\sigma'_3(t)$ and $S'_{31}(t)= \sigma'_3(t)-\sigma'_1(t)$ for one complete cycle.
- Evaluate stress intensity ranges ($\Delta S'_{ij}(t)$) and determine the maximum amongst all stress intensities and designate it as $\Delta S'_{rij}(t)$

$\Delta S'_{rij}=\max[|\Delta S'_{12}|,|\Delta S'_{23}|,|\Delta S'_{31}|]$.

- The alternating stress intensity (S_{alt}) for a reference time (t_o) is half of the maximum absolute stress intensity range ($\Delta S'_{rij}$).

In the Varying Principal Stress Directions procedure, the guidelines for choosing the reference time have not been specified. Therefore, it would be a rational approach to consider every point in one complete cycle as a reference point and the alternating stress intensity (S_{alt}) is largest value of the alternating stress intensities corresponding to all reference points.

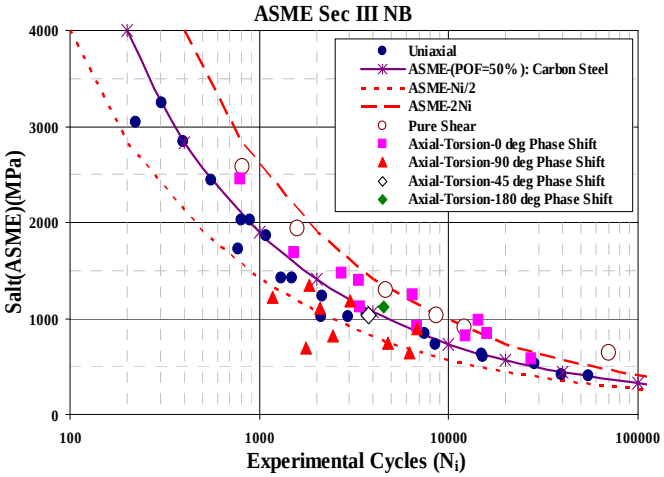

Fig. 11: Alternating stress intensity amplitude (S_{alt}) of ASME versus fatigue life for SA 333 Gr. 6

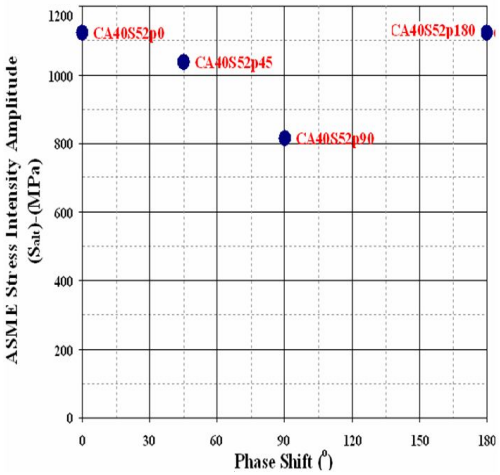

Fig. 12: The variation of ASME S_{alt} with phase shift

The alternating stress intensity amplitude (S_{alt}) has been evaluated for all tests as listed in table 3. The variation of S_{alt} with test life is plotted in Fig. 11. This Fig. indicates that the use of pure axial curve results in over-prediction of fatigue life for non-proportional loading conditions. However, the test life of a tube specimen under non-proportional load conditions is lesser than the corresponding test under proportional loading. Similarly, any invariant based life predicting criterion such as von-Mises or Rankine with stress/ strain equivalent parameter will result in over-prediction of fatigue life for non-proportional load condition.

As mentioned earlier, one set of tests were conducted to study the effect of phase shift under a given axial and shear strain amplitudes. These tests are CA40S52p0, CA40S52p45, CA40S52p90 and CA40S52p180. The procedure of ASME predicts minimum S_{alt} (or less fatigue damage) for 90^o phase shift case in comparison with the other phase shift cases (Fig. 12). However, it has been observed in the experimental studies that maximum damage occurs in case of 90^o phase shift axial-torsion test leading to shorter fatigue life. This calls for an urgent requirement to carry out fatigue studies under such loading scenario from the viewpoint of the phenomenological based damage such as critical plane approaches.

CONCLUSIONS

The multiaxial fatigue studies on SA 333 Gr. 6 material concludes that the strain-life curve as obtained from uniaxial tests is in agreement with the ASME best fit fatigue curve for carbon steel. The non-proportional fatigue loading causes extra material hardening leading to increase in fatigue damage in terms hysteresis loop area. The strain invariant based model/ ASME procedure (without use of safety factors) over-predicts fatigue life for non-proportional load conditions.

REFERENCES

[1] ASME Boiler & Pressure Vessel Code, Section III, American Society of Mechanical Engineers.
[2] C C Chu, "Fatigue damage calculations using the critical plane approach", *Journal of Engineering Materials and Technology*, 1995.
[3] D.L. Mc Diarmid, "A general criterion for high cycle multiaxial fatigue failure", *Fatigue of Engineering Materials*, 1991.
[4] D F Socie, "Multiaxial Fatigue Damage Models", *Journal of Engineering Materials and Technology*, 1987
[5] A Fatemi, D F Socie, "A critical plane approach to multiaxial fatigue damage including out-of-phase loading", *Fatigue Fracture of Engineering Materials Structures*, 1988.
[6] I.V. Papadopoulos, "A new criterion for fatigue strength for out-of-phase bending and torsion of hard metals", *International Journal of Fatigue*, 1994
[7] I.V. Papadopoulos, "Long life fatigue under multiaxial loading, *International Journal of Fatigue*, 2001.

[8] I.V. Papadopoulos, "A comparative study of multiaxial high cycle fatigue criteria for metals", *International Journal of Fatigue*, 1997.
[9] D. Ninic, "A stress-based multiaxial high cycle fatigue damage criterion", *International Journal of Fatigue*, 2006.
[10] Liu Xiaoshan, He Guoqui, Ding Xiangqun, Mo Defeng, Zhang Weihua, "Fatigue behavior and dislocation substructures for 6063 aluminum alloy under nonproportional loadings, International Journal of Fatigue 31 (2009) 1190–1195.